Available online at www.sciencedirect.com
SCIENCE DIRECT®
Journal of Solid State Chemistry 177 (2004) 2639–2643
JOURNAL OF SOLID STATE CHEMISTRY
http://elsevier.com/locate/jssc

The electronic structure of $Ba_{1-x}Ca_xTiO_3$ probed by X-ray absorption spectroscopy

K. Asokan,[a,*] J.C. Jan,[a] J.W. Chiou,[a] W.F. Pong,[a] M.-H. Tsai,[b] Y.K. Chang,[c] Y.Y. Chen,[c] H.H. Hsieh,[d] H.-J. Lin,[d] Y.W. Yang,[d] L.J. Lai,[d] and I.N. Lin[e]

[a] *Department of Physics, Tamkang University, Tamsui 251, Taiwan*
[b] *Department of Physics, National Sun Yat-Sen University, Kaohsiung 804, Taiwan*
[c] *Institute of Physics, Academia Sinica, Taipei 107, Taiwan*
[d] *National Synchrotron Radiation Research Center, Hsinchu 300, Taiwan*
[e] *Department of Materials Science and Engineering, Materials Science Center, National Tsing Hua University, Hsin-chu 300, Taiwan*

Received 10 December 2003; received in revised form 3 March 2004; accepted 25 April 2004

Abstract

We report O *K*-, Ca *K*- and $L_{3,2}$-, and Ti $L_{3,2}$-edge X-ray absorption near edge structure (XANES) spectra of $Ba_{1-x}Ca_xTiO_3$ ($x = 0$, 0.01, 0.08, and 1) and the electronic properties inferred from these XANES spectra. The spectra of O *K*-, Ca $L_{3,2}$- and Ti $L_{3,2}$-edges show characteristic spectral features attributable to the t_{2g} and e_g bands. The Ti and Ca $L_{3,2}$-edge spectra contain two sets of L_3 and L_2 features with a L_3–L_2 separation of about 5.5 and 3.4 eV, respectively. We also observe a pre-edge feature in the Ca *K*-edge spectra and drastically reduced t_{2g} features in the Ca $L_{3,2}$-edge spectra. Our XANES spectra reveal that the Ca 3*d* bands are low-lying and the Ca 3*d* t_{2g} bands are partially occupied.

PACS: 78.70.Dm; 71.20.−b; 77.84.−s

Keywords: XANES; Perovskites; Ferroelectric

1. Introduction

$BaTiO_3$ (hereafter referred to as BTO) is an ideal material for many technological applications owing to its controllable electrical properties over a wide range of mixed crystal formations and doping [1]. In BTO, the characteristic unit cell contains a highly polarizable TiO_6 octahedron. The collective polarization of TiO_6 octahedra was known to give rise to the ferroelectric property [1,2]. However, the origin of ferroelectricity and the nature of phase transitions in these perovskites remain elusive [3]. Previous extended X-ray absorption fine structure studies of ferroelectrics provided detailed quantitative information about the temperature dependence of the equilibrium properties and the Ti off-center displacement and clarified whether the phase transition was *an order–disorder or a displacive type* [4]. Alkaline-earth metals (AEMs), Ca, Sr and Ba, have been known to influence the basic structure, filled-space, and induced charge carriers in perovskites, which in turn influence a wide variety of physical properties such as magnetism, ferroelectricity, superconductivity, metal–insulator transition, and structural transformations [3,5]. Since ferro electric and structural properties depend on the electronic structure, X-ray absorption near edge structure (XANES) study of the electronic structures of these perovskites are useful. The measured Ti and Ca $L_{3,2}$-edge XANES spectra can elucidate the properties of the Ti and Ca 3*d* derived bands and the O and Ca *K*-edge spectra contain information about the couplings between cation 3*d* and O 2*p* orbitals in these perovskites [5]. We have studied $Ba_{1-x}Ca_xTiO_3$ only for $x = 0$ ($BaTiO_3$), 0.01, 0.08, and 1 ($CaTiO_3$, hereafter called as CTO).

2. Experimental

Details of preparation and characterization of the $Ba_{1-x}Ca_xTiO_3$ (0.01 and 0.08), BTO, and CTO samples

*Corresponding author. Fax: +91-1126893666.
E-mail address: asokan@nsc.ernet.in (K. Asokan).

0022-4596/$ - see front matter © 2004 Elsevier Inc. All rights reserved.
doi:10.1016/j.jssc.2004.04.043

have been reported elsewhere [6]. This work considers only $x \leqslant 0.08$ for the alloys because of the formation of the mixed phase in the intermediate compositions. All these samples' microstructures were done using optical microscope and their chemical analysis by Energy Dispersive X-ray analysis (EDX). EDX was carried out by taking on an average of 3–4 different areas of the samples. These results indicated that the composition were consistent with expected stoichiometry for the composition of Ca = 1% and 8% [6]. Room temperature XANES measurements were obtained at various beamlines, as specified below, of the National Synchrotron Radiation Research Center (NSRRC), Hsinchu, Taiwan running with an electron beam energy of 1.5 GeV and a maximum stored current of 200 mA. The O and Ca *K*-edge spectra were measured at the high-energy spherical grating monochromator beamline (HSGM) and at the Si(111) double crystal monochromator beamline (DCM), respectively. Both were measured in the fluorescence mode using a seven-element Ge detector. Measurements of the Ca and Ti $L_{3,2}$-edges were obtained in sample drain current mode at the wide-range spherical grating monochromator beamline (WSGM) and the Dragon beamlines, respectively. The energy scale was calibrated using those of the reference TiO_2 (for O *K*-edge [7] and Ti $L_{3,2}$-edge [8]) and CaO (for Ca *K*-edge [9] and $L_{3,2}$-edge [10]) samples reported earlier. Typical resolutions of these spectra were ~0.2 eV for HSGM, WSGM, and Dragon and ~0.7 eV for DCM beamlines.

3. Results and discussion

Fig. 1 shows the O *K*-edge XANES spectra of $Ba_{1-x}Ca_xTiO_3$ with $x = 0.01$ and 0.08, BTO, CTO, and TiO_2 [11]. These spectra are normalized to the same area in the energy range between 550 and 570 eV (not fully shown in the figure). The O *K*-edge XANES spectra basically reflect transitions from the O 1*s* core-state to the unoccupied O 2*p*-derived states, which are hybridized states with the relatively narrow 3*d* and broader 4*sp* bands of the 3*d*-transition metal (TM) ions and the AEM bands. The features marked by A_1 to E_1 in the spectrum of CTO are centered at ~531, 534, 537, 540, and 544 eV, respectively. Inset in Fig. 1 shows a magnified view, in which the background intensity was subtracted out by a best-fitted Gaussian curve, to better resolve features A_1 and B_1. These two peaks are best resolved for TiO_2 and not well-resolved for $Ba_{1-x}Ca_xTiO_3$. Similar two-peak structures at the threshold of the O *K*-edges were observed for other 3*d*-TM oxides [12]. The two-peak structure near the threshold can be attributed dominantly to the hybridization with the Ti 3*d* orbitals. Peaks A_1 and B_1 for $Ba_{1-x}Ca_xTiO_3$ have a separation of about 2 eV, which is

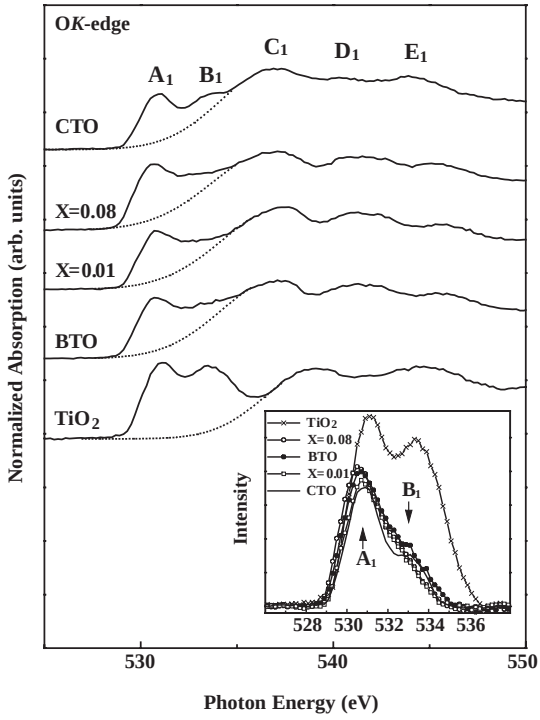

Fig. 1. Normalized O *K*-edge XANES spectra of $Ba_{1-x}Ca_xTiO_3$ ($x = 0.01$ and 0.08), BTO, CTO, and TiO_2. The dashed line is a best-fitted Gaussian background. The region of features A_1 and B_1 after subtraction by the background is magnified in the inset.

similar to that of two-peak structure near the threshold of the TiO_2 spectrum with a splitting of ~2.5 eV. Peaks A_1 and B_1 can be attributed to the anti-bonding states between O 2*p* and Ti t_{2g} and e_g orbitals, respectively [13]. The Ti e_g orbitals are directed toward the O ions and thus their coupling with O 2*p* orbitals are stronger, so that their anti-bonding hybridized states are at higher energies than those of the t_{2g} orbitals. The intensity of features A_1 and B_1 remain roughly constant for all compositions of $Ba_{1-x}Ca_xTiO_3$. Feature B_1 is drastically reduced for $Ba_{1-x}Ca_xTiO_3$ relative to that for TiO_2. The areas under features A_1 and B_1 for $Ba_{1-x}Ca_xTiO_3$ are much smaller than that for TiO_2, which indicates that the introduction of AEMs reduces the number of unoccupied O 2*p*–Ti 3*d* anti-bonding states. In other words, the presence of AEMs reduces the O 2*p*–Ti 3*d* coupling. This is because AEMs have smaller electronegativity (1.00 for Ca and 0.89 for Ba) than Ti (1.54) [14], so that there is an electronic charge transfer from AEMs to Ti, which raises the Ti 3*d* orbital energy. Since O 2*p* orbitals couple more strongly with Ti e_g orbitals, the intensity of B_1 is reduced more than that of A_1. The reduction of both A_1 and B_1 relative to that of TiO_2 shows enhancement of the effective charge on the O ions in $Ba_{1-x}Ca_xTiO_3$, BTO and CTO. Feature C_1 is due to the O 2*p* derived states that are hybridized with the Ba 5*d* or Ca 3*d* orbitals, while features D_1 and E_1 are due to

the O 2*p* and/or 3*p* derived states that are hybridized with the Ti and AEM higher-energy *sp* states [13].

Fig. 2 shows the normalized Ca *K*-edge XANES spectra of $Ba_{1-x}Ca_xTiO_3$ ($x = 0.01$ and 0.08), CTO, and CaO, in which the five major features are denoted as A_2 to E_2. These features vary with the Ca concentration indicating a change in the local environment and/or a charge transfer at the Ca site. The inset in the figure highlights the increase of the spectral intensity of the pre-edge feature A_2 with the Ca concentration. This pre-edge feature corresponds to the excitation of the Ca 1*s* electron into the unoccupied Ca 3*d*–O 2*p* hybridized states, which have substantial *p*-orbital components at the Ca site. Such a transition is allowed for the Ca ion with a tetrahedral symmetry and is normally characterized by a strong peak. A similar pre-edge feature at the Ca *K*-edge was reported for CaF_2 and some garnets [9,15,16]. The change in the intensity of the pre-edge feature A_2 in the Ca *K*-edge spectra, as shown in the inset of Fig. 2, can be understood from the nearest neighbor (NN) oxygen arrangement. In BTO, the Ba ion is coordinated with 12 O ions and hence the substitutional Ca ion in $Ba_{1-x}Ca_xTiO_3$ has a similar coordination number. This large coordination number favors the coupling of the quadruply directional Ca 3*d* orbitals with neighboring O 2*p* orbitals. This Ca 3*d*–O 2*p* hybridized band is broadened to extend below the valence band maximum (VBM), because the dominant

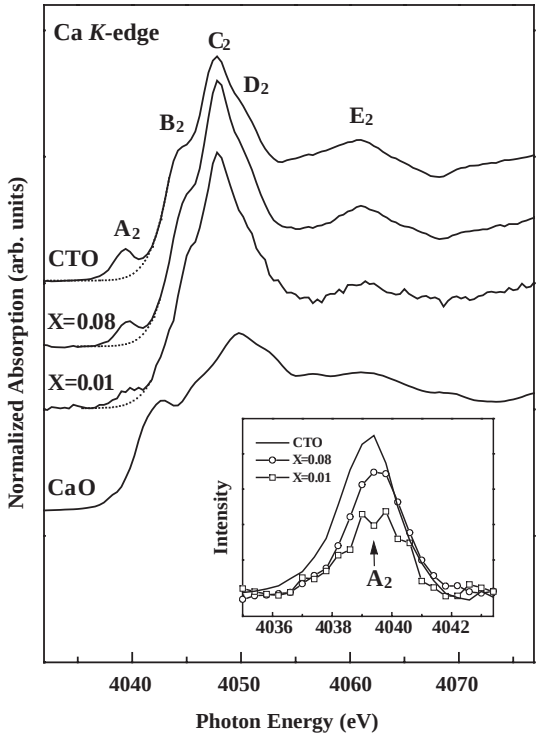

Fig. 2. Normalized Ca *K*-edge XANES spectra of $Ba_{1-x}Ca_xTiO_3$ ($x = 0.01$ and 0.08), BTO, CTO, and CaO. The dashed line is a best-fitted Gaussian background. The region of feature A_2 after subtraction by the background is magnified in the inset.

part of the 2*p* band of oxides is known to be in the valence band. Thus, although an isolated Ca atom has a $3d$ electronic configuration of $3d^0$, i.e. 3*d* orbitals are empty, a Ca ion in the oxides can have a configuration strongly mixed with the charged $3d^1\underline{L}$ configuration by covalent hybridization [17,18], where $\underline{L}$ stands for a hole in the anion valence-band. The Ca 3*d* derived states below the Fermi level gain charge from O 2*p* orbitals, which gives rise to holes and contributes to A_2. The 3*d* TM *K*-edge XANES showed that A_2 contained information about the number of holes [19]. Thus, the intensity of A_2 is related to the amount of hole doping. The change in the intensity of A_2 can be used as a common measure of the hole concentration in perovskites. The features within $\sim$10 eV of the edge threshold correspond to electronic transitions from the Ca 1*s* core state to the unoccupied Ca 4*p* derived-states, which are hybridized strongly with O 2*p* orbitals. These features are sensitive to the crystal field giving rise by the O ions surrounding the Ca ion [16,19,20]. The calculated partial density of Ca 4*p* states [13] showed that features C_2 and D_2 are dominated by the Ca 4*p* derived states, while feature B_2 is primarily contributed by O 2*p*–Ca 4*p* hybridized states. Feature E_2 is contributed by the unoccupied Ca 5*p* states [13]. The position of E_2 does not differ significantly from that of CaO. The physical reason is that the high-energy Ca 5*p* orbitals are much more extended than the 4*p* orbitals, so that the details of the local environment at the Ca site is not important. That is why E_2 is much broader than C_2.

Fig. 3 presents XANES spectra of $Ba_{1-x}Ca_xTiO_3$ ($x = 0.01$, and 0.08), BTO, CTO, and TiO_2 at the Ti $L_{3,2}$-edges. These spectra are split into L_3 and L_2 regions by the spin–orbit interaction [10,21–24], with a separation of $\sim$5.5 eV. Each region contains t_{2g} and e_g splitting of about 2 eV due to the crystal-field effect. The observed t_{2g}–e_g splitting agrees well with the spin-polarized first-principles calculation of 2.1 eV [25]. The similarity in the Ti $L_{3,2}$-edge spectra of $Ba_{1-x}Ca_xTiO_3$, BTO and CTO suggests that the ground states of the Ti ions in these oxides are similar. These spectra contain four dominant peaks of which the first two peaks, A_3 and B_3, correspond to the L_3 edge with t_{2g} and e_g symmetries, respectively. The other two peaks, C_3 and D_3, in the higher energy region correspond to the L_2 edge with t_{2g} and e_g symmetries, respectively [23,26]. The small leading structures (marked by the vertical arrows) below the first main peak was attributed either to a part of the p^5d^1 multiplet [21] or to the anisotropy in the local electron structure caused by the screening effect of the core-hole potential [26]. The spectra exhibit a chemical shift with respect to that of the reference compound TiO_2. Although there is a negative shift of $\sim$0.2 eV of the L_3-edge t_{2g} peak for BTO and $Ba_{1-x}Ca_xTiO_3$ (except CTO) with respect to that for TiO_2, the position of the L_2t_{2g} peak does not show any significant shift (as shown

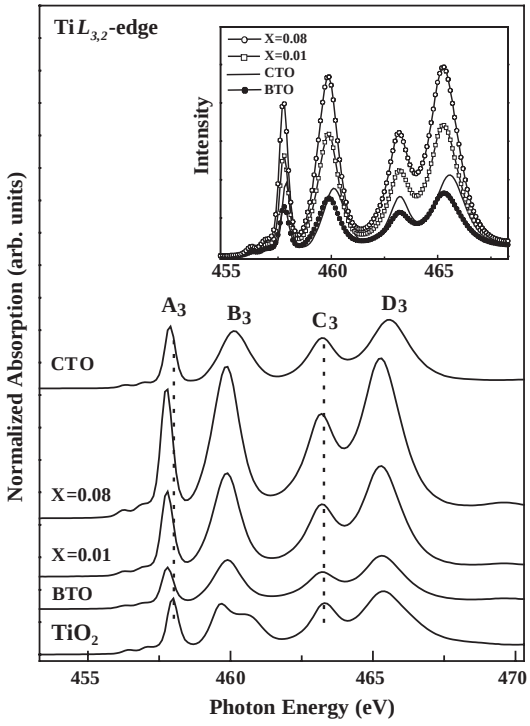

Fig. 3. Normalized Ti $L_{3,2}$-edge XANES spectra of $Ba_{1-x}Ca_xTiO_3$ ($x = 0.01$ and 0.08), BTO, CTO, and TiO_2. The vertical dashed lines are used to show the shifts in the peak positions relative to those of the reference TiO_2.

by the dotted lines). The relative intensities of t_{2g} and e_g peaks are determined by the degree of covalent mixing in the ground state and the numbers of t_{2g} and e_g orbitals. Note that there are two e_g orbitals and three t_{2g} orbitals. That is why the area under B_3 is larger than that under A_3. The intensities of the Ti $L_{3,2}$-edge features increase with x for the $x \leqslant 0.08$ samples considered in this study, as shown in the inset of Fig. 3, though it decreases for large x. This finding shows that the substitution of Ba by Ca increases the number of Ti 3*d* holes.

It is evident from the figure that there is an energy shift of ~ 0.35 eV both in L_3 and L_2 edges of e_g orbitals if one compares CTO and BTO. This shift is due to varying local environment of Ba^{2+} and Ca^{2+} ions. Even though the number of valence electrons both Ba and Ca ions are the same, substitution of Ba by Ca will significantly influence the structure owing to different ionic radii of Ca and Ba ions. Hence change in the structural parameters leading to change in electronic structures of CTO and BTO. In other words, this shift is ascribed to the fact that the electron affinity (negative value) of the Ba^{2+} ions is less than that of Ca^{2+} ions; thus the bonding strength between cations and anions is changed when Ca^{2+} ions are doped into BTO [6].

The Ca $L_{3,2}$-edges XANES spectra of $Ba_{1-x}Ca_xTiO_3$ with $x = 0.01$ and 0.08, CTO, and CaO are shown in Fig. 4. The major features in the Ca $L_{3,2}$-edge spectra are dominated by the Ca $2p \rightarrow 3d$ transitions. Similar to the Ti $L_{3,2}$-edge spectra, the features in Fig. 4 can be attributed dominantly to the spin–orbit splitting of the Ca $2p_{1/2}$ and $2p_{3/2}$ core states and the splitting of the 3*d* t_{2g} and e_g orbitals due to the crystal-field of surrounding NN O ions [10,21–23]. The L_3- and L_2-edge separation due to the $2p_{3/2}$–$2p_{1/2}$ core-level splitting is about 3.4 eV. According to the numbers of orbitals of the t_{2g} and e_g symmetry as stated in the previous paragraph, the integrated intensity of $A_4(C_4)$, i.e. the area under $A_4(C_4)$, would be about 3/2 larger than that of $B_4(D_4)$. However, Fig. 4 shows that the intensities of L_3t_{2g} feature A_4 and L_2t_{2g} feature C_4, respectively, are greatly reduced relative to those of L_3e_g feature B_4 and L_2e_g feature D_4. These results are very different from those of Ti $L_{3,2}$-edge spectra. Features A_4 and C_4 are still noticeable for CaO. However, they are drastically reduced for $Ba_{1-x}Ca_xTiO_3$ and CTO. In conjunction with the Ca *K*-edge result stated previously, the drastic reduction of features A_4 and C_4 can be attributed to the low-lying Ca 3*d* derived bands, in which the t_{2g} bands become dominantly occupied. This interpretation is supported by the spin-polarized first-principles calculations for $Ba_{1-x}Sr_xTiO_3$, which show that a dominant part of the t_{2g} bands of AEMs, i.e. Ba and Sr, lies below VBM [25]. The ions in BTO and CTO are usually thought to be fully ionized Ba^{2+}, Ca^{2+}, Ti^{4+} and O^{2-} ions. This study shows that these ions are not fully ionized. Fig. 4 shows that the XANES spectra of CTO and $Ba_{1-x}Ca_xTiO_3$ ($x = 0.01$ and 0.08) have slight chemical shifts toward

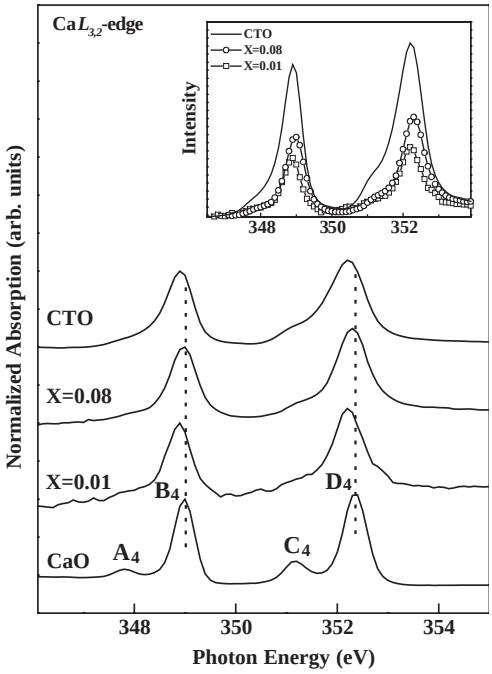

Fig. 4. Normalized Ca $L_{3,2}$-edge XANES spectra of $Ba_{1-x}Ca_xTiO_3$ ($x = 0.01$ and 0.08), CTO, and CaO. The vertical dashed lines are used to show the shifts in the peak positions relative to those of the reference CaO.

the lower energy side relative to that of CaO (as shown by the dotted lines). The inset in Fig. 4 shows that the intensities of the Ca $L_{3,2}$-edge features increase with the Ca concentration. Similar trend is also observed for A_2 shown in the inset of Fig. 2.

4. Conclusions

We have measured O *K*-, Ca *K*- and $L_{3,2}$-, and Ti $L_{3,2}$-edge XANES spectra of $Ba_{1-x}Ca_xTiO_3$ with $x = 0, 0.01$, 0.08, and 1 and obtained the electronic structures of these ferroelectrics. The spectra of O *K*-, Ca $L_{3,2}$- and Ti $L_{3,2}$-edges show characteristic spectral features attributable to the t_{2g} and e_g bands. The Ti $L_{3,2}$-edge spectra contain two sets of L_3 and L_2 features resulted from transitions from Ti $2p_{1/2}$ and $2p_{3/2}$ core states to the unoccupied Ti 3*d* bands with a L_3–L_2 separation of about 5.5 eV. The L_3–L_2 separation observed in the Ca $L_{3,2}$-edge spectra is about 3.4 eV. We observe a pre-edge feature in the Ca *K*-edge spectra and drastically reduced t_{2g} features in the Ca $L_{3,2}$-edge spectra. Our XANES spectra show that Ca 3*d* bands are low-lying and the Ca 3*d* t_{2g} bands are partially occupied.

Acknowledgments

The authors (K.A. and W.F.P.) would like to thank the National Science Council of the Republic of China for financially supporting this research under Contract No. NSC-92-2112-M-032-025. One of us (K.A.) would also like to thank the director of the Nuclear Science Center, New Delhi (India) for granting him leave and offering encouragements. The excellent cooperation of the NSRRC staff is greatly appreciated.

References

[1] M.E. Lines, A.M. Glass, Principles and Applications of Ferroelectrics and Related Materials, Oxford University Press, Oxford, 1977.
[2] C. Kittel, Introduction to Solid State Physics, Wiley, New York, 1996.
[3] R.E. Cohen, Nature 359 (1992) 136;
R.E. Cohen (Ed.), Fundamental Physics of Ferroelectrics, AIP Proceedings, 2000.
[4] B. Ravel, Ferroelectric Phase Transitions in Oxide Perovskites Studied by XAFS, Ph.D. Thesis, University of Washington, 1997.
[5] M. Imada, A. Fujimori, Y. Tokura, Rev. Mod. Phys. 70 (1998) 1039.
[6] T.F. Lin, C.T. Hu, I.N. Lin, J. Appl. Phys. 67 (1990) 1042.
[7] R. Brydson, H. Sauer, W. Engel, J.M. Thomas, E. Zeither, N. Kosugi, H. Kuroda, J. Phys.: Condens. Mater. 1 (1989) 797.
[8] R.S. Liu, Y.C. Cheng, J.M. Chen, R.G. Liu, J.L. Wang, J.C.T sai, M.Y. Hsu, Mater. Lett. 37 (1998) 285.
[9] C. Sogiura, Jpn. J. Appl. Phys. 31 (1992) 2816.
[10] F.J. Himpsel, U.O. Karlsson, A.B. Mclean, L.J. Terminello, F.M.F. de Groot, M. Abbate, J.C. Fuggle, J.A. Yarmoff, B.T. Thole, G.A. Sawatzky, Phys. Rev. B 43 (1991) 6899.
[11] K. Asokan, J.C. Jan, J.W. Chiou, W.F. Pong, P.K. Tseng, I.N. Lin, J. Synchrotron Radiation 8 (2001) 839–841.
[12] F.M.F. de Groot, M. Grioni, J.C. Fuggle, J. Ghijsen, G.A. Sawatzky, H. Petersen, Phys. Rev. B 40 (1989) 5715;
F.M.F. de Groot, J. Faber, M. Michiels, M.T. Czyzyk, M. Abbate, J.C. Fuggle, Phys. Rev. B 48 (1993) 2074.
[13] K. Asokan, J.C. Jan, J.W. Chiou, W.F. Pong, M.-H. Tsai, H.L. Shih, H.Y. Chen, H.C. Hsueh, C.C. Chuang, Y.K. Chang, Y.Y. Chen, I.N. Lin, J. Phys.: Condens. Matter 13 (2001) 11087.
[14] Table of Periodic Properties of the Elements, Sargent-Welch Scientific, Skokie, Illinois, 1980.
[15] J. Chaboy, S. Quartieri, Phys. Rev. B 52 (1995) 6349.
[16] J.H. Barkyoumb, A.N. Mansour, Phys. Rev. B 46 (1992) 8768.
[17] T. Tiedje, K.M. Colbow, D. Rogers, W. Eberhardt, Phy. Rev. Lett. 65 (1990) 1243.
[18] K. Ueda, H. Yangi, H. Hosono, H. Kawazoc, J. Phys.: Condens. Matter 11 (1999) 3545.
[19] B. Ravel, E.A. Stern, Physica B 208 and 209 (1995) 316.
[20] J. Garcia, J. Blasco, M.G. Proietti, M. Benfatto, Phys. Rev. B 52 (1995) 15823.
[21] F.M.F. de Groot, J.C. Fuggle, B.T. Thole, G.A. Sawatzky, Phys. Rev. B 41 (1990) 928.
[22] M. Abbate, R. Potze, G.A. Sawatzky, C. Schlenker, H.J. Lin, L.H. Tjeng, C.T. Chen, D. Teehan, T.S. Turner, Phys. Rev. B 51 (1995) 10150.
[23] J.P. Crocombette, F. Jollet, J. Phys.: Condens. Matter 6 (1994) 10811.
[24] P.O. Nilsson, G. Forssell, Phys. Rev. B 16 (1977) 3352.
[25] M.-H. Tsai, Private communication.
[26] G. van der Laan, Phys. Rev. B 41 (1990) 12366.